EARTHQUAKE ENGINEERING AND STRUCTURAL DYNAMICS, VOL. 25, 1353–1371 (1996)

ON LINEAR-SATURATION (LS) CONTROL OF BUILDINGS

J. MONGKOL*, BINOD K. BHARTIA† AND YOZO FUJINO‡

Department of Civil Engineering, The University of Tokyo, Hongo 7-3-1, Bunkyo-ku, Tokyo 113, Japan

SUMMARY

This paper proposes the Linear-Saturation (LS) control as a new and suitable control algorithm for buildings with an Active Mass Damper (AMD) system. It takes into account the physical constraints on the AMD system and uncertainties in the loading. The LS control consists of a low-gain linear control when the system is close to the zero state and bang-bang control otherwise. This paper provides a precise formulation of the saturation control and presents optimal solutions which can be implemented in the state space. A numerical scheme to synthesize the switching surface which is needed to implement the bang-bang control is developed. Furthermore, a method to demarcate the region for linear control is proposed. The effectiveness of the LS control is verified through numerical simulations with one- and multi-storey buildings subjected to earthquakes. It is shown that the LS control provides better performance compared to even the gain-scheduled LQ control.

KEY WORDS: active mass damper; active tuned mass damper; non-linear control; saturation control; actuator limitation

1. INTRODUCTION

Active control has emerged as a new structural control technology. It has found already a number of applications mostly in Japan. It has been used, for example, to reduce the responses of tall buildings and bridge towers against natural loads like windstorms and earthquakes.

Kobori and Minai[1] in 1956 and Yao[2] in 1972 were among the first researchers to have drawn the attention of the civil engineers to the potential uses of active control. A much needed multi-disciplinary research to develop the actual uses, however, started only in mid-1980s. Since then, we have identified several unique requirements of the active control for structures, and consequently a number of control hardwares and algorithms have been developed. Previews of state-of-the-art can be found in, among others, Soong[3] and Fujino *et al.*[4]

Tendon control,[5] variable stiffness control,[6] and Active Mass Damper[7] (AMD) are some of the control mechanisms developed and studied widely. Among these, the AMD system, consisting of an auxiliary mass attached to the controlled structure through parallel placed spring, damper and actuator, has proved the most popular in real applications.[4]

This paper seeks a suitable control algorithm for controlling buildings with AMD system. So far, most of the popularly used control algorithms have belonged to the class of linear controls with fixed gains. The examples include LQ control, pole allocation, H^∞ control. These controls have seemed to be a natural choice in the sense that the controlled buildings themselves are usually modelled as linear systems. There are other important angles to this problem, however, which have not received enough attention.

Natural dynamic loads of interest in civil engineering such as wind and earthquake excitations occur once in a while and last for only a short duration. A control system used during these load events is thus used only

* Ph.D. Candidate
† Associate Professor
‡ Professor

CCC 0098–8847/96/121353–19

Received 28 February 1995
Revised 3 June 1996

occasionally. The intensity of these load events is very much random. It varies from event to event and also during an event. Amidst the above load uncertainty, the control system must operate always within its physical constraints such as the inherent bounds on control force, control power and stroke length, which are governed by the control hardware.

After considering the above scenario, we found that a linear control with fixed gain is not suitable for our problem, for the following reasons:

(1) Since the control force is the linear function of the responses, the control system is effective, or is used fully, during a certain load type with a narrow load intensity range only. In a severe case such as strong earthquake when the required control force exceeds the limit, the control system must be shut down to save the actuator itself.
(2) Such a control is not compatible with the occasional, or emergency, nature of our control needs. Often our concern is to reduce the peak responses, and with certain control system given, we should rather use it fully to achieve our purpose. But, by its very nature, a linear control tries to modify the controlled system and achieves a balance between the reduction in "average" response measures and the demand on the control system.

2. NON-LINEAR CONTROLS

Some modified linear controls and some non-linear controls which address to some extent the above raised issues have been proposed. Some of these controls are discussed below. Then, we propose a new control algorithm called the linear-saturation (LS) control.

(1) Optimum Pulse Control: This control which was proposed by Masri *et al.*[8,9] applies the pulse forces in the proper direction and timing through actuators located on the structure. A gas pulse generator with variable intensity was used as a control force. The control scheme is simple yet very effective. As known, almost all the active control system implemented so far is the hybrid type (tuned mass damper with an actuator) with a fixed gain (Reference 4). The present study aims at full usage of the actuator in the conventional hybrid mass damper. Therefore, in this context, use of pulse control proposed by Masri *et al.*[8,9] is not within the scope of the study although it is effective.
(2) Gain-Scheduled Linear Control: This control uses different gains from among a set of pre-selected gains in accordance to the load type and intensity, which in turn are inferred from the response measures. Fujita *et al.*[10] use such a control against wind loads where one of the three gains — low, medium, or high — is used depending upon the acceleration response of the structure and stroke length of the actuator. Being a linear, though time-varying, control, this control is quite appealing. However, designing a proper set of control gains and selecting an indicator for the gain switchings requires a laborious effort.
(3) Sliding Mode Control: This control has lately drawn a lot of attention.[11,12] It is said to possess a high degree of robustness against uncertainities in system parameters as well as loading. However, there are a number of issues, for example, relating to the choice of sliding surface, control chattering, imposing the constraints, etc., which remain to be fully explored.
(4) Nonlinear Feedback Control: Here we refer to a control where the control force is a non-linear function of the responses. It aims to induce selective non-linearities into the controlled system so as to achieve the desired performance. Wu *et al.*[13] use such a control where control force is a polynomial function of the state variables. The effectiveness or otherwise of this control is not yet clear.

Over the next three sections, we develop the proposed linear-saturation control. First we discuss the saturation control in Section 3. Then we show that the saturation control needs to be coupled with a linear control, hence the proposed name, the linear-saturation control of Section 4. We conclude with some simulation results in Section 5.

3. SATURATION CONTROL

In saturation control, instead of indirectly using the penalty on control force to specify the control force constraint as in case of LQ control, we explicitly impose the constraint on control force. Examples of this control method include minimum-time control, minimum-fuel control, etc. Johnson[14] studied the saturation control and showed that it consists of two control modes: singular control, which is used when the controlled system lies on the so-called singular surface, and bang-bang control, wherein the control force takes only the extreme values. He outlined a procedure to obtain the optimal solutions. Letov,[15] Chang,[16] Desoer,[17] and others too have studied similar control problems. All solution procedures available in the literature so far, however, are very restrictive . These have not been able to yield optimal solutions for other than trivial problems. More recently, Higashihara and Indrawan[18] have studied a similar bounded control.

The saturation control is not yet widely used in applications of control engineers because it was difficult to implement the bang-bang control[7] with available actuators. However, with the new advances in actuators, especially with the linear motor or the force-controlled AC servo-motor actuators, it is no longer difficult to implement the bang-bang control. Therefore, in light of its appropriateness for our problem, this paper advocates once again the use of the saturation control. This paper provides a precise formulation of the saturation control and presents optimal solutions valid for arbitrary order systems.

3.1. Formulation of saturation control

Let us consider an m-storey building with an AMD system installed at the roof. Figure 1 shows a schematic diagram of the building—AMD system. It is common to model the building–AMD system as having $m + 1$ degrees of freedom and to choose the displacements and velocities at m stories and auxiliary mass as constituting the state variables. The equations of motion of the building–AMD system, assumed to be linear and time invariant, may be written as

$$\dot{\mathbf{x}}(t) = \mathbf{A}\mathbf{x}(t) + \mathbf{b}u(t), \quad \mathbf{x}(0) = \mathbf{x}_0 \tag{1}$$

where $\mathbf{x} = [x_1 \ x_2 \ \cdots \ x_n]^T$ is the $n = 2(m + 1)$-state vector, u is the scalar control force, $\mathbf{A}$ is the system matrix, and $\mathbf{b}$ is the control input vector. In equation (1), we have considered an initial disturbance problem, and have assumed that no external disturbance is present. In the sequel, we first formulate the saturation

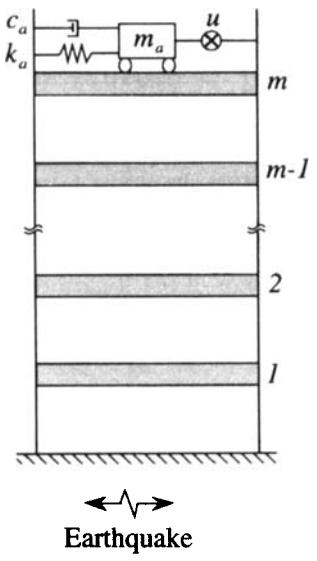

Figure 1. An m-storey building with AMD system at the roof

control with initial disturbance only. Later on, we propose modifications needed when external disturbances too are present.

An AMD system, depending on its hardware, must conform to a number of inequality constraints. These constraints may be of the following types:

$$|u(t)| \leqslant u_c \tag{2}$$

$$g_i[\mathbf{x}(t), u(t)] \leqslant 0, \quad i = 1, \ldots, n_1 \tag{3}$$

$$\int_0^{t_f} g_i[\mathbf{x}(t), u(t)]\, dt \leqslant 0, \quad i = n_1 + 1, \ldots, n_2 \tag{4}$$

Equation (2) specifies u_c as the bound on control force. Equation (3) includes constraints on state variables, for example, bounds on stroke length, control power, etc. Equation (4) denotes integral (or cumulative) constraints, for example, a bound on control energy.

We apply the control force u to bring the building–AMD system from initial state x_0 to zero state at time t_f, that is,

$$\mathbf{x}(t_f) = 0 \tag{5}$$

where t_f is the terminal (or final) time. We choose u following the optimal control approach. It involves choosing u so as to minimize a certain performance index and satisfying simultaneously the equations of motion, the boundary conditions and the constraints, as given in equations (1)–(5).

If we consider a performance index which is at the most a linear function in u, consider the constraint given in equation (2) only, and let t_f be not fixed, but to be optimized by control itself, then we obtain a control referred to as the saturation control, our focus here. Since the constraints in equations (3) and (4) are equally important, in the last section we indicate two approaches to satisfy them.

As the performance index, denoted here by J, we choose the time integral of a quadratic function of $\mathbf{x}$, namely

$$J = \frac{1}{2} \int_0^{t_f} \mathbf{x}^T(t) \mathbf{Q} \mathbf{x}(t)\, dt \tag{6}$$

in which $\mathbf{Q}$, a positive semi-definite weighting matrix, specifies relative importances given to reducing the different state variables. This performance index is similar to the one used in the LQ control:

$$J = \frac{1}{2} \int_0^{t_f} (\mathbf{x}^T(t) \mathbf{Q} \mathbf{x}(t) + ru^2)\, dt \tag{7a}$$

The only difference between equations (6) and (7a) is that the former puts no penalty on the control force. For latter purpose, we note that optimal LQ control, assuming $t_f \to \infty$, is given as

$$u(t) = -r^{-1} \mathbf{b}^T \mathbf{K} \mathbf{x}(t) = \mathbf{g}^T \mathbf{x}(t), \tag{7b}$$

where $\mathbf{g}$ is the gain vector and $\mathbf{K}$ is the solution of the Ricatti equation

$$0 = \mathbf{A}^T \mathbf{K} + \mathbf{K} \mathbf{A} + \mathbf{Q} - \mathbf{K} \mathbf{b} r^{-1} \mathbf{b}^T \mathbf{K}. \tag{7c}$$

3.2. Optimal solution of saturation control

We obtain the optimal solution following the approach of Pontryagin's maximum principle, which is a variational principle and states that an optimal control must maximize a given function known as the Hamiltonian. We leave readers to find the details of the derivation of the necessary conditions in Reference 19 or 20 and present here the main results only. For our purpose, the Hamiltonian function H is defined as

$$H(\mathbf{x}, \mathbf{p}, u) = -\tfrac{1}{2} \mathbf{x}^T \mathbf{Q} \mathbf{x} + \mathbf{p}^T (\mathbf{A} \mathbf{x} + \mathbf{b} u) \tag{8}$$

wherein, on the right, first term is the integrand of the performance index and second term in brackets is the right-hand side of the equations of motion. The vector $\mathbf{p}$ is an n-vector of Lagrange's multipliers known as the co-state vector. Then, denoting the optimal control as $u^*(t) = u^*[\mathbf{x}(t), \mathbf{p}(t)]$, the necessary conditions for optimal control are as follows:

$$\dot{\mathbf{x}} = \frac{\partial H^*(\mathbf{x}, \mathbf{p}, u^*)}{\partial \mathbf{p}} = \mathbf{A}\mathbf{x} + \mathbf{b}u^* \tag{9}$$

$$\dot{\mathbf{p}} = \frac{\partial H^*(\mathbf{x}, \mathbf{p}, u^*)}{\partial \mathbf{x}} = \mathbf{Q}\mathbf{x} - \mathbf{A}^{\mathrm{T}}\mathbf{p} \tag{10}$$

$$H^*[\mathbf{x}(t), \mathbf{p}(t), u^*(t)] = \max_{|u(t)| \leq u_c} H[\mathbf{x}(t), \mathbf{p}(t), u(t)] \tag{11}$$

and

$$H^*[\mathbf{x}(t_f), \mathbf{p}(t_f), u^*(t_f)]\delta t_f - \mathbf{p}^{\mathrm{T}}(t_f)\delta\mathbf{x}(t_f) = 0 \tag{12}$$

Equation (9) ensures that the optimal control and the optimal trajectory satisfy the equations of motion. Equation (10) represents the co-state equation and results from the variational principle. Equations (9) and (10) together are called the canonical equations. Their joint boundary conditions are as given in equations (1) and (5). Equation (11) ensures that the optimal control maximizes the Hamiltonian. Equation (12), also known as the transversality condition, specifies the boundary conditions at the terminal time t_f. Since $\mathbf{x}(t_f)$ is required to be zero, its variation $\delta\mathbf{x}(t_f)$ must be zero. Thus, the second term in equation (12) becomes zero and $\mathbf{p}(t_f)$ remains arbitrary. Furthermore, since t_f is not fixed, δt_f is not zero, and therefore,

$$H^*(t_f) = H^*[\mathbf{x}(t_f), \mathbf{p}(t_f), u^*(t_f)] = 0 \tag{13}$$

Equation (13) yields optimal value for t_f.

With respect to equations (11) and (8), two cases are possible. One is when $\phi(t) = \mathbf{b}^{\mathrm{T}}\mathbf{p}(t) = 0$ holds for a finite time. In this case, H becomes independent of u, and consequently, equation (11) becomes irrelevant in obtaining the optimal control. This case is called the singular case. For this case, the optimal control, denoted herein as $u_s(t)$, is obtained as follows. Since $\phi(t) = 0$ holds for a finite time, it implies that the time derivatives of $\phi(t)$ would also be zero:

$$0 = \phi(t) = \dot{\phi}(t) = \ddot{\phi}(t) = \cdots \tag{14}$$

On repeated substitutions of equations (9) and (10), we obtain

$$0 = \dot{\phi}(t) = \mathbf{b}^{\mathrm{T}}\dot{\mathbf{p}}(t) = \mathbf{b}^{\mathrm{T}}(\mathbf{Q}\mathbf{x} - \mathbf{A}^{\mathrm{T}}\mathbf{p}) \tag{15}$$

and

$$0 = \ddot{\phi}(t) = \mathbf{b}^{\mathrm{T}}(\mathbf{Q}\dot{\mathbf{x}} - \mathbf{A}^{\mathrm{T}}\dot{\mathbf{p}}) = \mathbf{b}^{\mathrm{T}}\mathbf{Q}(\mathbf{A}\mathbf{x} + \mathbf{b}u) - \mathbf{b}^{\mathrm{T}}\mathbf{A}^{\mathrm{T}}(\mathbf{Q}\mathbf{x} - \mathbf{A}^{\mathrm{T}}\mathbf{p}) \tag{16}$$

Given $\mathbf{b}^{\mathrm{T}}\mathbf{Q}\mathbf{b} \neq 0$, we can solve equation (16) to obtain

$$u_s(t) = -(\mathbf{b}^{\mathrm{T}}\mathbf{Q}\mathbf{b})^{-1}\mathbf{b}^{\mathrm{T}}[(\mathbf{Q}\mathbf{A} - \mathbf{A}^{\mathrm{T}}\mathbf{Q})\mathbf{x} + \mathbf{A}^{\mathrm{T}}\mathbf{A}^{\mathrm{T}}\mathbf{p}] \tag{17}$$

The second case (termed the normal case) is when $\phi(t) = \mathbf{b}^{\mathrm{T}}\mathbf{p}(t) \neq 0$. Then, equation (11) yields the optimal control, denoted herein as $u_b(t)$, as

$$u_b(t) = u_c \operatorname{sgn}[\mathbf{b}^{\mathrm{T}}\mathbf{p}(t)] \tag{18}$$

which is a bang-bang control.

Thus, the saturation control is a dual mode control, consisting of the singular control u_s and the bang-bang control u_b. It is seen from equations (17) and (18) that the optimal solutions depend also on $\mathbf{p}$. In the following, we seek the optimal solutions in terms of $\mathbf{x}$ only so as to facilitate the control implementation.

3.2.1. Optimal singular control. Wonham and Johnson[21] show that for linear systems optimal singular control is a linear control. Indeed, it can be obtained as the asymptotic solution of the LQ control as the

control force weight r approaches zero. Friedland[22] provides this solution, though in a different context. Following Friedland, the relationship is given by

$$u_s(t) = -\mathbf{b}^{\#}\mathbf{A}\mathbf{x}(t) \tag{19}$$

in which $\mathbf{b}^{\#}$, a row-vector, is the left inverse of $\mathbf{b}$; i.e. $\mathbf{b}^{\#}\mathbf{b} = 1$. The vector $\mathbf{b}^{\#}$ is given by the formula

$$\mathbf{b}^{\#} = (\mathbf{b}^{\mathrm{T}}\mathbf{Q}\mathbf{b})^{-1}\mathbf{b}^{\mathrm{T}}(\mathbf{Q} + \mathbf{A}^{\mathrm{T}}\mathbf{M}) \tag{20}$$

in which $\mathbf{M}$ is the solution of the Riccati equation

$$\mathbf{0} = \bar{\mathbf{A}}^{\mathrm{T}}\mathbf{M} + \mathbf{M}\bar{\mathbf{A}} + \mathbf{Q} - \mathbf{Q}\gamma\mathbf{Q} - \mathbf{M}\mathbf{A}\gamma\mathbf{A}^{\mathrm{T}}\mathbf{M} \tag{21}$$

where $\gamma = \mathbf{b}(\mathbf{b}^{\mathrm{T}}\mathbf{Q}\mathbf{b})$ and $\mathbf{A} = \mathbf{A}(\mathbf{I} - \gamma\mathbf{Q})$, in which $\mathbf{I}$ is an identity matrix. The matrix $\mathbf{M}$ also satisfies the relation $\mathbf{M}\mathbf{b} = \mathbf{0}$.

Since the optimal singular control is a linear control, the $\mathbf{p}$ and $\mathbf{x}$ vectors during this control are related linearly. Their relationship is given by

$$\mathbf{p}(t) = -\mathbf{M}\mathbf{x}(t) \tag{22}$$

We recall the fact that during the singular control $\phi(t) = \mathbf{b}^{\mathrm{T}}\mathbf{p}(t) = 0$ holds identically. We can show that $\mathbf{b}^{\mathrm{T}}\mathbf{p} = 0$ is equivalent to the relation

$$\mathbf{b}^{\#}\mathbf{x} = 0 \tag{23}$$

Equation (23) describes a linear hypersurface. During singular control the controlled system always lies on this surface. This surface accordingly is called the singular surface.

Since $u_s(t)$ must also be bounded by u_c, it restricts the domain of singular surface in which $u_s(t)$ can be used. In other words, for singular control purposes, the singular surface defined in equation (23) has boundaries, which following equations (2) and (19) are

$$|\mathbf{b}^{\#}\mathbf{A}\mathbf{x}| \leqslant u_c \tag{24}$$

We prove that the solutions of u_s given in equations (17) and (19) are equivalent. On expanding and rearranging the terms, equation (21) becomes

$$\mathbf{0} = \mathbf{A}^{\mathrm{T}}\mathbf{M} + \mathbf{M}\mathbf{A} + \mathbf{Q} - (\mathbf{Q} + \mathbf{M}\mathbf{A})\mathbf{b}\mathbf{b}^{\#} \tag{21a}$$

On post-multiplying it on both sides by $\mathbf{x}$, and since on singualr surface, $\mathbf{b}^{\#}\mathbf{x} = 0$, we obtain

$$\mathbf{0} = (\mathbf{A}^{\mathrm{T}}\mathbf{M} + \mathbf{Q})\mathbf{x} + \mathbf{M}\mathbf{A}\mathbf{x} \tag{21b}$$

Putting equation (22) into equation (17) gives

$$u_s(t) = -(\mathbf{b}^{\mathrm{T}}\mathbf{Q}\mathbf{b})^{-1}\mathbf{b}^{\mathrm{T}}[\mathbf{Q}\mathbf{A}\mathbf{x} - \mathbf{A}^{\mathrm{T}}(\mathbf{Q} + \mathbf{A}^{\mathrm{T}}\mathbf{M})\mathbf{x}] \tag{17a}$$

which, on substitution from equation (21b), proves the desired relation:

$$u_s(t) = -(\mathbf{b}^{\mathrm{T}}\mathbf{Q}\mathbf{b})^{-1}\mathbf{b}^{\mathrm{T}}[\mathbf{Q}\mathbf{A}\mathbf{x} + \mathbf{M}\mathbf{A}\mathbf{x}] = -\mathbf{b}^{\#}\mathbf{A}\mathbf{x}$$

Example. Consider a Single-Degree-of-Freedom (SDOF) system with the equation of motion

(E1) $$\ddot{y} + 2\omega_0\xi\dot{y} + \omega_0^2 y = u/m$$

where m is the mass, ω_0 is the undamped natural frequency, ξ is the damping ratio, and u is the control force. Using $\mathbf{x} = [x_1 \;\; x_2]^{\mathrm{T}} = [y \;\; \dot{y}]^{\mathrm{T}}$ as the state vector, equation (E1) is rewritten as

(E2) $$\dot{\mathbf{x}} = \mathbf{A}\mathbf{x} + \mathbf{b}\mathbf{u} = \begin{bmatrix} 0 & 1 \\ -\omega_0^2 & -2\omega_0\xi \end{bmatrix}\begin{bmatrix} x_1 \\ x_2 \end{bmatrix} + \begin{bmatrix} 0 \\ 1/m \end{bmatrix} u$$

Denoting the co-state vector $\mathbf{p} = [p_1 \;\; p_2]^{\mathrm{T}}$, the singular control is used whenever

(E3) $$0 = \mathbf{b}^{\mathrm{T}}\mathbf{p}(t) = p_2(t)$$

By letting $\mathbf{Q} = \text{diag}\{q_1 \ q_2\}$, from equations (21) and (22) we have

(E4) $$\mathbf{M} = \begin{bmatrix} \sqrt{q_1 q_2} & 0 \\ 0 & 0 \end{bmatrix}$$

(E5) $$\mathbf{b}^{\#} = [m\sqrt{q_1/q_2} \ \ m]$$

Thus, the singular surface is

(E6) $$0 = \mathbf{b}^{\#}\mathbf{x} = \sqrt{q_1}x_1 + \sqrt{q_2}x_2$$

and the optimal singular control is

(E7) $$u_s = -\mathbf{b}^{\#}\mathbf{A}\mathbf{x} = \omega_0^2 m x_1 + 2\omega_0 \xi m x_2 - m\sqrt{q_1/q_2}\,x_2$$

The boundary of the singular surface is

(E8) $$x_2 = -\sqrt{q_1/q_2}\,x_1 \quad \text{and} \quad |x_1| \leqslant \frac{u_c}{m(q_1/q_2 + \omega_0^2 + 2\omega_0\xi\sqrt{q_1/q_2})}$$

3.2.2. Optimal bang-bang control. We seek to reduce the solution of optimal bang-bang control given in equation (18) into the state feedback form. In principle, it is possible. One can solve the necessary conditions given in equations (9)–(12) seeking a relationship between **p** and **x**. This relationship, however, is often obtained in the form of a set of non-linear, implicit functions. Thus, the reduction task is quite formidable. Moreover, this approach often does not work with systems having more than three states.[18]

This paper abandons finding an explicit relationship between **p** and **x**. Instead, it seeks to find the switching surface, which, as explained below, proves sufficient to implement the bang-bang control in the state space.

3.3. Switching surface

Given an initial state $\mathbf{x}_0$, in the state space there is a set of fixed points where the bang-bang control switches its sign. Accordingly, these points are called the switching points. The collection of all switching points constitutes a continuous, non-linear hypersurface. On this hypersurface, the function $\phi(t)$, also called the switching function, is zero. Since $\phi(t)$ is zero also on the singular surface, the two surfaces join together smoothly at the boundary of the singular surface. The combined surface thus obtained is called the switching surface which seperates the state space by half and pass through the origin as will be shown later.

Once the switching surface is obtained, implementing the saturation control is straightforward: if the system lies on the singular surface, optimal control is the singular control given by equation (19); otherwise, optimal control is the bang-bang control with u at $+u_c$ or $-u_c$ depending upon on which side of the switching surface the system is.

Obtaining the switching surface analytically is again very difficult. This paper proposes a numerical scheme to obtain the same.

3.3.1. Method of backward integration. A typical control force time history during the saturation control of a linear system consists of initially a few cycles of the bang-bang control, which brings the system from initial state $\mathbf{x}_0$ onto the singular surface, followed by the singular control, which makes the system slide on the singular surface to the origin.

We make use of the above knowledge about the control force time history to generate the switching points via the backward integrations of the canonical equations. We begin the backward integration of equations (9) and (10) from a point $x(0)$ on the singular surface, where $\mathbf{p}(0) = -\mathbf{M}\mathbf{x}(0)$ too would be known, with the control force u at $+u_c$ or $-u_c$. We monitor the values of state vector $\mathbf{x}(t)$ and switching function $\phi(t) = \mathbf{b}^{\mathrm{T}}\mathbf{p}(t)$. Suppose that at time $t = \tau_1$, $\phi(\tau_1)$ becomes zero. Then, in accordance to equation (18), the forward bang-bang control would have changed its sign at point $\mathbf{x}(\tau_1)$. Thus the point $\mathbf{x}(\tau_1)$ is a switching point. We switch the sign of u from $\pm u_c$ to $\mp u_c$ and continue the backward integration further. As in the

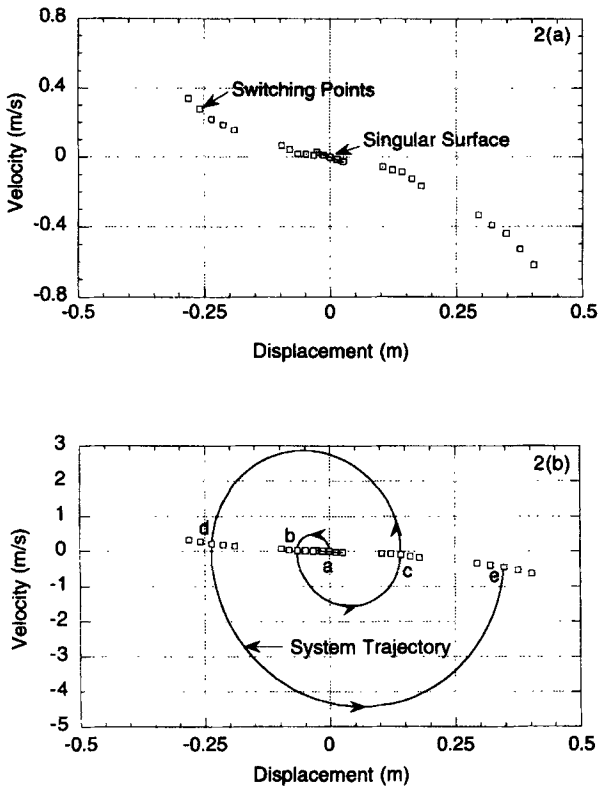

Figure 2. Singular surface, system trajectory and switching points for a SDOF system

above, we can generate further switching points, where each successive switching point would be farther away from the origin. We can repeat the above integration process starting from different points on the singular surface, and each time generate a distinct set of switching points.

We illustrate the backward integration procedure through an example. As in the Example, a SDOF system controlled by an external control force is considered, with $m = 7{\cdot}45$ kg, $\omega = 2{\cdot}44$ Hz, $\xi = 1\%$, $u_c = 50$ N, and $\mathbf{Q} = \text{diag}[1\ 1]$. Following the solutions given in the Example, we obtain the singular line and its boundaries, as shown in Figure 2(a). The singular line is discretized at five points, from where we begin the backward integrations with a time step of five milliseconds and generate four switching points each. Thus a total of twenty switching points are generated. A typical system trajectory obtained starting from the zero state, or point a, is shown in Figure 2(b), which yields the switching points b, c, d, and e.

Once we have generated enough switching points, we fit a surface through them. The fitted surface approximates the switching surface. This paper proposes to use a polynomial function to approximate the switching surface.

3.3.2. Polynomial switching surface. Let us denote the switching surface by the function $s(\mathbf{x}) = 0$. Since the switching surface is symmetric about the origin, $s(\mathbf{x})$ must be an odd function: i.e. $s(\mathbf{x}) = -s(-\mathbf{x})$. The literature known to the authors does not provide any information on the functional forms suitable for $s(\mathbf{x})$. Therefore, because of its simplicity, this paper approximates $s(\mathbf{x})$ by polynomial functions.

A polynomial function of $\mathbf{x}$ will normally contain also terms which would be even functions. For example, letting $\mathbf{x}$ be $\mathbf{x} = [x_1\ x_2]^T$ a normal polynomial function of $\mathbf{x}$ would be

$$0 = -x_1 + a_1 x_2 + a_2 x_2^2 + a_3 x_2^3 + \cdots \tag{25}$$

wherein $a_1, a_2, a_3, \ldots$ are the polynomial coefficients. We see in equation (25) that the term $a_2 x_2^2$ is an even function. We must modify such terms into suitable odd functions. For example, $a_2 x_2^2$ can be modified into $a_2|x_2|x_2$. Thus, for a system with two states, we choose $s(\mathbf{x})$ as

$$0 = s(\mathbf{x}) = -x_1 + a_1 x_2 + a_2|x_2|x_2 + a_3 x_2^3 + a_4|x_2^3|x_2 + a_5 x_2^5 + a_6|x_2^5|x_2 + \cdots \tag{26}$$

For a system with four states, i.e. $\mathbf{x} = [x_1 \ x_2 \ x_3 \ x_4]^T$, a normal polynomial function of $\mathbf{x}$ would contain terms like $x_2x_3, x_2x_3x_4$, etc. The term x_2x_3 is an even function. It can be substituted by two terms, $|x_2|x_3$ and $|x_3|x_2$. The term $x_2x_3x_4$ is an odd function. But still it can be substituted by four odd function terms; namely, $|x_2x_3|x_4$, $|x_2x_4|x_3$, $|x_3x_4|x_2$ and $x_2x_3x_4$. We see that when $\mathbf{x}$ is of size greater than two, there is an arbitrariness involved in converting or replacing the polynomial terms. For $\mathbf{x}$ of size four, we choose $s(\mathbf{x})$ as

$$\begin{aligned} 0 = s(\mathbf{x}) = {} & -x_1 + a_1x_2 + a_2x_3 + a_3x_4 + a_4|x_2|x_2 + a_5|x_3|x_2 + a_6|x_4|x_2 + a_7|x_2|x_3 \\ & + a_8|x_3|x_3 + a_9|x_4|x_3 + a_{10}|x_2|x_4 + a_{11}|x_3|x_4 + a_{12}|x_4|x_4 + a_{13}x_2^3 \\ & + a_{14}|x_2x_3|x_2 + a_{15}|x_2x_4|x_2 + a_{16}x_3^2x_2 + a_{17}|x_3x_4|x_2 + a_{18}x_4^2x_2 + a_{19}x_2^2x_3 \\ & + a_{20}|x_2x_3|x_3 + a_{21}|x_2x_4|x_3 + a_{22}x_3^3 + a_{23}|x_3x_4|x_3 + a_{24}x_4^2x_3 + a_{25}x_2^2x_4 \\ & + a_{26}|x_2x_3|x_4 + a_{27}|x_2x_4|x_4 + a_{28}x_3^2x_4 + a_{29}|x_3x_4|x_4 + a_{30}x_4^3 + \cdots . \end{aligned} \tag{27}$$

For a polynomial of third order, equation (27) contains 30 coefficients.

We determine the polynomial coefficients by fitting the surface to the generated switching points. To obtain the best fit we use the least square error as the criterion. We note that the switching surface can be very non-linear in the vicinity of the boundary of the singular surface.[23] Also, as explained in the next section, we do not use (or need) the switching surface near the origin. Therefore, while fitting the surface we usually do not consider the points on the singular surface as well as the switching points close to the origin.

As an example, we fit equation (26) to the switching points shown in Figure 2. We chose not to consider the points on the singular line as well as the first switching points, e.g. points *a* and *b*. Thus the surface is fitted to a total of 15 switching points. The best fit is found to be a sixth order polynomial:

$$0 = s(\mathbf{x}) = -x_1 + 2{\cdot}6x_2 + 16{\cdot}5|x_2|x_2 + 68{\cdot}2x_2^3 + 150{\cdot}0|x_2^3|x_2 + 169{\cdot}6x_2^5 + 72{\cdot}9|x_2^5|x_2.$$

4. LINEAR-SATURATION (LS) CONTROL

We have so far focused on the saturation control of systems with initial disturbance only. The developed control scheme needs to be modified if external disturbances too are present.

In the initial disturbance case as the system approaches the zero state (or origin), it rides onto the singular surface and slides, during which the control force being linear gradually becomes zero. A similar time history for the control force is not obtained if an external disturbance too is present. This is because the external disturbance prevents the system from remaining on the singular surface. As a result, even near the origin, the present control scheme applies the bang-bang control, which may lead, in turn, to the induced motion in the system, and consequently, to control chattering.

To overcome the control chattering problem this paper proposes to demarcate a small region in state space centered at the origin within which a low-gain linear control should be used. This modification has prompted the proposed name: the linear-saturation control. In the next section we propose a method to demarcate the linear control region.

4.1. Design of linear control region

We first choose the linear control to be used, which may be designed following any standard control algorithm. Suppose that the chosen linear control is

$$u_l(t) = \mathbf{g}_l^T \mathbf{x}(t) \tag{28}$$

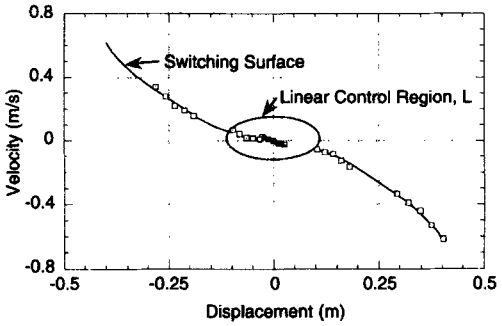

Figure 3. Switching surface and linear control region for a SDOF system

wherein the subscript l stands for the linear control, and $\mathbf{g}_l$ denotes the column vector of control gains. To demarcate the linear control region, we use an energy-based criterion. To this end, we let $\mathbf{x}$ be so arranged that $\mathbf{x} = [\mathbf{y}^T \ \dot{\mathbf{y}}^T]^T$, where $\mathbf{y}$ and $\dot{\mathbf{y}}$, respectively, denote the vectors of displacements and velocities, $\hat{\mathbf{M}}$ and $\hat{\mathbf{K}}$, respectively, denote the mass and stiffness matrices. Then, the total energy of the system, denoted by $E(x)$, may be written as

$$E(\mathbf{x}) = \tfrac{1}{2}\mathbf{y}^T\hat{\mathbf{K}}\mathbf{y} + \tfrac{1}{2}\dot{\mathbf{y}}^T\hat{\mathbf{M}}\dot{\mathbf{y}} \tag{29}$$

which is the sum of the potential and kinetic energies. Letting $\mathbf{g}_l$ be as $\mathbf{g}_l = [\mathbf{g}_{l1}^T \ \mathbf{g}_{l2}^T]^T$, and letting $\mathbf{g}_{l1}$ and $\mathbf{g}_{l2}$, respectively, denote the vectors of gains with respect to displacements and velocities, we can rewrite equation (28) as

$$u_l(t) = \mathbf{g}_{l1}^T\mathbf{y}(t) + \mathbf{g}_{l2}^T\dot{\mathbf{y}}(t) \tag{28a}$$

We choose the linear control region, denoted by L, as

$$L = \{\mathbf{x} : E(\mathbf{x}) \leqslant e\} \tag{30}$$

Thus, L, a subset of $\mathbf{x}$, is an ellipsoid, whose size (or volume) depends on the value of e. Since $u_l(t)$ too must be bounded by u_c, the region L must be enclosed within the two following parallel surfaces: $\mathbf{g}_l^T\mathbf{x} = +u_c$ and $\mathbf{g}_l^T\mathbf{x} = -u_c$. Accordingly, e is computed as the minimum value of $E(\mathbf{x})$ such that the corresponding $\mathbf{x}$ satisfies $|\mathbf{g}_l^T\mathbf{x}| = u_c$. From equations (29) and (28a) using the constraint in equation (30), we can obtain e as

$$e = \tfrac{1}{2}u_c^2(\mathbf{g}_{l1}^T\hat{\mathbf{K}}^{-1}\mathbf{g}_{l1} + \mathbf{g}_{l2}^T\hat{\mathbf{M}}^{-1}\mathbf{g}_{l2})^{-1} \tag{31}$$

Thus L depends on u_c and $\mathbf{g}_l$ values as well as $\hat{\mathbf{M}}$ and $\hat{\mathbf{K}}$. Increasing u_c leads to a larger L. Similarly, decreasing the control gains leads to a larger L, and vice versa. Usually, we choose L large enough so that it encloses the whole singular surface as well as the switching points close to the zero state. As a result, the saturation control, to be performed outside of L only, reduces to the bang-bang control only.

From the Example problem in Section 3.2.1, Figure 3 shows the switching surface and a typical linear control region. The region L encloses the singular line as well as the first switching points.

In summary, the proposed LS control is as follows:

$$u(t) = \begin{cases} u_l(t) & \text{if } \mathbf{x} \in L; \\ u_b(t) & \text{otherwise} \end{cases} \tag{32}$$

in which $u_l(t)$ is as given in equation (28), and $u_b(t)$, based on the switching surface approach, is $u_b(t) = u_c \operatorname{sgn}[s(\mathbf{x})]$.

We note that a proper design of L is very crucial in preventing the control chattering, which occurs mainly when the system is close to the intersection of the region L and the switching surface.

5. SIMULATION RESULTS

A number of simulations, all with respect to earthquake loads, with one- and fifty-four-storey buildings, both provided with AMD systems at the roof, have been performed to verify the characteristics and performance of the LS control. We bring out its two main features: one, its adaptiveness to respond to the load events of a wide load intensity range and the other, its superior control performance owing to its full use of the actuator capacity via the bang-bang control.

5.1. Case of one-storey building

We consider one-storey building with AMD system at the roof, as in Figure 1. The one-storey building may be a reduced order model, for example, a first-mode-only model of a multi-storey building. We assume following values for the structural parameters: building mass, $m = 750$ kg; building stiffness, $k = 1{\cdot}76 \times 10^5$ N/m; and damping ratio $\xi = c/2\sqrt{km} = 1$ per cent.

The AMD system is designed as follows. Its auxiliary mass m_a equals 7·45 kg, which is roughly 1 per cent of the building mass. For its stiffness k_a, we consider two cases: one is, $k_a = 1{\cdot}72 \times 10^3$ N/m, in which case $\sqrt{k_a/m_a} \cong \sqrt{k/m}$, which leads to the auxiliary mass being tuned to the building; and another is, $k_a = 1{\cdot}72 \times 10^2$ N/m, which value is one-tenth of the first value. For both cases of k_a, we choose $\xi_a = c_a/2\sqrt{k_a m_a} = 6$ per cent, which is roughly the value of optimal damping ratio for the first case. Henceforth, the first case is referred to as the active tuned mass damper (ATMD), and the second case simply as AMD. The value of the bound on control force, u_c, is assumed in both cases to be 50 N.

5.1.1. Case of one-storey building with AMD. The system of one-storey building and the AMD system consist of four states: namely, displacement of building, denoted as x_1; displacement of auxiliary mass, denoted as x_2; velocity of building, denoted as x_3; and velocity of auxiliary mass, denoted as x_4. Denoting the state vector by $\mathbf{x} = [x_1\ x_2\ x_3\ x_4]^T$, we can write the equations of motion of the building–AMD system subjected to an horizontal earthquake loading as

$$\dot{\mathbf{x}} = \mathbf{A}\mathbf{x} + \mathbf{b}u + \mathbf{f}\ddot{x}_0 = \begin{bmatrix} 0 & 0 & 1 & 0 \\ 0 & 0 & 0 & 1 \\ -\dfrac{k+k_a}{m} & \dfrac{k_a}{m} & -\dfrac{c+c_a}{m} & \dfrac{c_a}{m} \\ \dfrac{k_a}{m_a} & -\dfrac{k_a}{m_a} & \dfrac{c_a}{m_a} & -\dfrac{c_a}{m_a} \end{bmatrix} \begin{bmatrix} x_1 \\ x_2 \\ x_3 \\ x_4 \end{bmatrix} + \begin{bmatrix} 0 \\ 0 \\ \dfrac{1}{m} \\ -\dfrac{1}{m_a} \end{bmatrix} u + \begin{bmatrix} 0 \\ 0 \\ -1 \\ -1 \end{bmatrix} \ddot{x}_0 \tag{33}$$

where $\mathbf{f}$ is the input vector and ddot $\mathbf{x}_0$ is the ground acceleration.

To obtain the LS control algorithm, we first design the saturation control, followed by the design of the coupled linear control. The weight matrix $\mathbf{Q}$ in equation (6) is assumed as $\mathbf{Q} = \operatorname{diag}\{0\ 0\ 1\ 0\}$, which puts a unit weight on x_3 only. Solving equations (20) and (21) with $\mathbf{A}$ and $\mathbf{b}$ taken from equation (33) yields an expression for the singular surface as defined in equation (23). The boundary of the singular surface is defined by equation (24). We discretize the singular surface and perform the backward integrations of equations (9) and (10) to generate the switching points. Then a polynomial surface of the type given in equation (27) is fitted to approximate the switching surface. It is found that a third-order polynomial provides the best fit. To see the matching between the fitted surface and the switching points, we plot in Figure 4 the value of x_1 estimated from equation (27) vs. the actual values of x_1 for all switching points. The plot thus obtained is

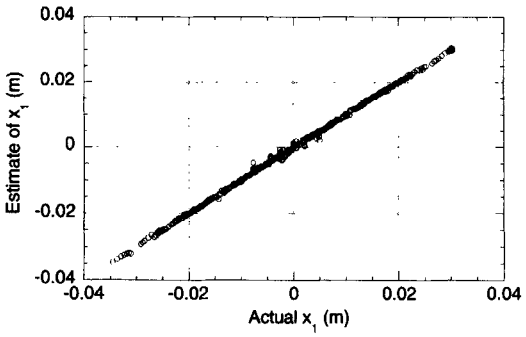

Figure 4. Matching between switching points and fitted switching surface

seen to be a straight line with unit slope, which shows that the fitted surface approximates the switching surface well.

The coupled linear control u_l is assumed to be an LQ control. The gain vector $\mathbf{g}_l$ is obtained from equation (7b) with $\mathbf{Q} = \text{diag}\{0\ 0{\cdot}1\ 1\ 0\}$ and $r = 3{\cdot}0 \times 10^{-6}$. r is obtained from equation (31) and the Riccati equation of equations (7b) and (7c). Therefore, it is guaranteed that the control limit is not exceeded when the control switches to linear control when the energy level is below e. The linear control region L is obtained by solving equations (31) and (30).

The simulations are performed with two standard recorded earthquake motions, namely the El Centro(NS) and Taft(EW) ground acceleration records scaled to the different peak ground acceleration (PGA) values. In all cases, we compare the performance of the LS control with that of a Gain-Scheduled LQ (GSLQ) control. As explained in Section 2, the GSLQ control is designed to use a different gain vector for each ground motion and each PGA value so that the control force is always bounded by u_c. In other words, for a large PGA value, the control gains would be smaller, and vice versa. The gains for the GSLQ control are obtained from equation (7b) with the weight matrix $\mathbf{Q} = \text{diag}\{0\ 0{\cdot}1\ 1\ 0\}$ and the r value adjusted according to the ground motion and the PGA value.

Subject to the El Centro motion with PGA at 250 gal, the peak displacement response of the building with no control is 2·07 cm. Figure 5(a) shows the time history of the ground acceleration and Figure 5(b) shows the time history of the displacement response. With the LS control, the peak displacement response reduces by 23 per cent, to 1·60 cm. Figures 5(c) and 5(e), respectively, show the reduced displacement response, the relative displacement of the auxiliary mass (i.e. stroke length), and the control force. It is seen that the control force consists of both bang-bang and linear controls. To study the adaptive feature of the LS control, we perform simulations with different PGA values. Figures 6(a) and 6(b) show the control force time histories for PGA values at 150 and 250 gal s. This figure makes clear that as the PGA value (or load intensity) increases, the LS control applies the bang-bang control more often, and vice versa.

In Figure 7, we plot the performance curves. Figure 7(a) shows the reduction in the peak value of x_1, Figure 7(b) shows the reduction in the Root Mean Square (RMS) value of x_1, and Figure 7(c) shows the peak stroke length, all plotted vs. PGA values. The performance curves are plotted for the LS control as well as the GSLQ control. It is seen that the LS control outperforms the GSLQ control, though the stroke length is larger. Put differently, it implies that the LS control can provide a similar control performance as the GSLQ control by using less powerful actuators.

5.1.2. Case of one-storey building with ATMD. Since this case differs only slightly from the case of AMD, we present only the performance curves and some control force time histories. The matrix $\mathbf{Q}$ in equation (6) is assumed to be $\mathbf{Q} = \text{diag}\{0\ 1\ 1\ 0\}$. The linear control u_l is again an LQ control whose gains are obtained from equation (7b) with $r = 2{\cdot}0 \times 10^{-6}$ and $\mathbf{Q} = \text{diag}\{0\ 1\ 1\ 0\}$. The GSLQ control uses $\mathbf{Q} = \text{diag}\{0\ 1\ 1\ 0\}$ and the r value is adjusted according to the ground motion and the PGA value. More weight of the added mass displacement in matrix $\mathbf{Q}$ is necessary in case of ATMD since

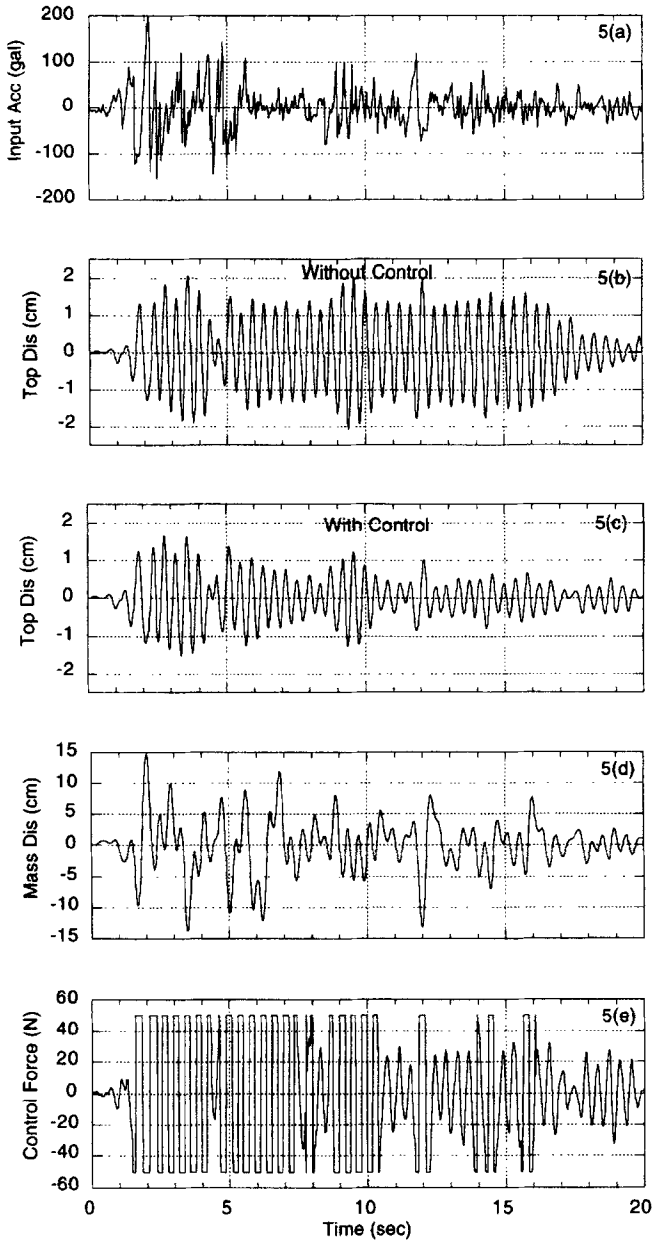

Figure 5. Input, response, and control force for a SDOF system with AMD subjected to the El Centro ground motion at PGA 250 gal

the ATMD stroke length is large due to its closely spaced natural frequency characteristic. Figure 8 shows the performance curves. It is again seen that the LS control provides larger response reductions compared with the GSLQ control. Figure 9 shows the time histories of control forces for PGA values at 150 and 250 gals.

We now discuss the effect of the linear control u_l. If u_l and the linear control region L are designed properly, it should prevent control chattering, which otherwise occurs in the neighbourhood of zero response. Figure 6, which corresponds to the AMD case, shows that the control chattering is almost absent.

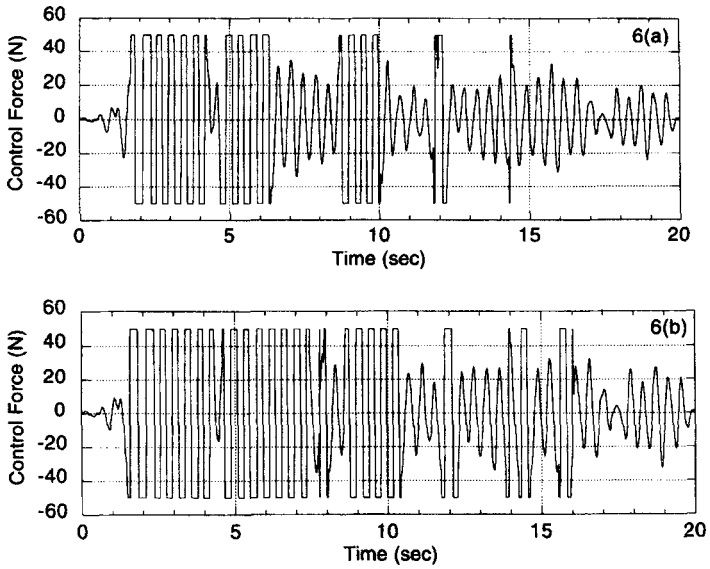

Figure 6. Control forces for a SDOF system with AMD subjected to the El Centro ground motion with PGA values at (a) 150 and (b) 250 gal s

Figure 9, which corresponds to the ATMD case, however, shows the instances of control chattering. The control chattering occurs less often as the PGA value is increased, for then the system remains away from the origin longer. We note that there is a trade-off involved between the control performance and preventing the control chattering.

5.2. *Case of a tall building with AMD*

We consider a 54-storey tall building, whose first two modal periods are 5·67 and 2·17 s, and whose modal damping ratios are 1 per cent for all modes. Subject to the El Centro motion with PGA at 100 gal, the peak displacement response at the top storey is 15·05 cm, to which the first mode contributes 67 per cent, the second mode contributes 30 per cent, and the rest comes from the higher modes. We assume an AMD system at the roof, consisting of $m_a = 3{\cdot}9 \times 10^5$ kg, $h_a = 1$ per cent, and $k_a = 4{\cdot}80 \times 10^4$ N/m set as small as 10 per cent of the tuned value of ATMD. Finally, we assume u_c at 200 kN.

We design the LS control as follows. The bang-bang control is performed based on the responses of the auxiliary mass and top storey only. The switching surface to implement the bang-bang control is obtained with respect to a system consisting of the AMD system and the first-mode-only model of the building. In other words, we design a bang-bang control with output feedback. The linear control u_l is designed to be an LQ control with the state feedback. The GSLQ control too, performed for comparison purposes, is designed to be a state feedback control.

With respect to the El Centro motion, Figure 10 shows the time histories of the displacement responses at the top storey with and without control when the PGA value equals 100 gal, and the control forces when the PGA values equal 100 and 200 gal s. Figure 11 shows the performance curves. Even though GSLQ is slightly better for small excitation, it is seen that the LS control outperforms the GSLQ control, this despite the fact that the LS control has been performed with the output feedback (or reduced order model). Also, despite the presence of significant motion in the second mode, the LS control does not cause any evident spillover.

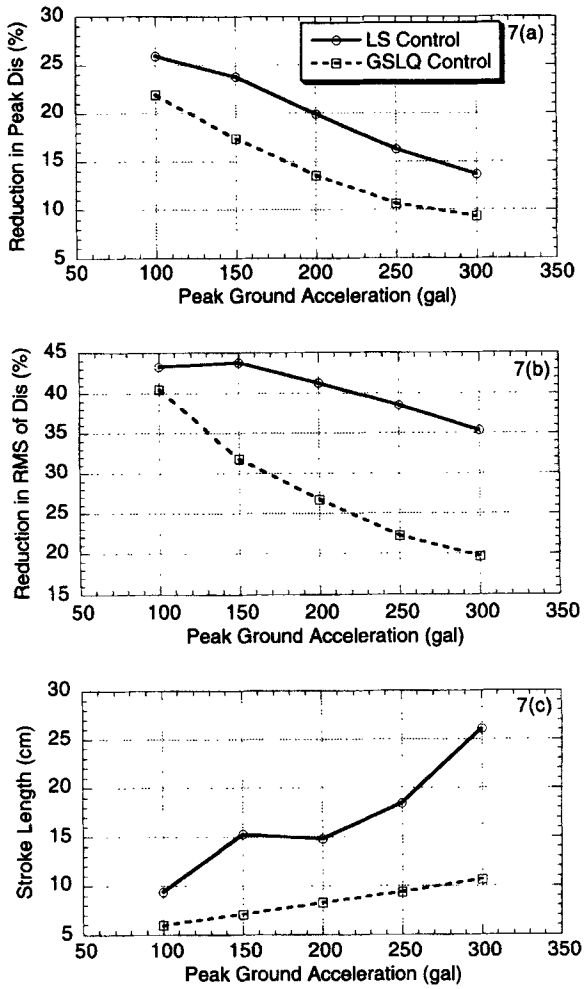

Figure 7. Performance curves for a SDOF system with AMD subjected to the El Centro ground motion

6. SUMMARY AND DISCUSSIONS

This paper proposes the LS control as a suitable control for buildings with AMD system. It presents a precise formulation of the saturation control and provides optimal solutions which can be implemented in the state space. The paper implements saturation control in order to deal with the control capacity limitation in the presence of unpredictable external disturbances like windstorms and earthquakes. The saturation control is coupled by a low-gain linear control in the near field to prevent the control chattering due to the presence of noise. Through simulations under earthquake excitations, it shows that the LS control outperforms the gain-scheduled LQ control. On a cautionary note, a number of problems remain as discussed below.

The problem of control chattering is found in the closely spaced system as in case of ATMD. More investigations should be done on development of LS control for a closely spaced system. The extension to the multiple control force case is needed to control the coupled lateral-torsional motion of tall buildings. Obtaining the switching surface which is important in the LS control, unfortunately, becomes more and more complex as the size of the state vector increases. There are two approaches to

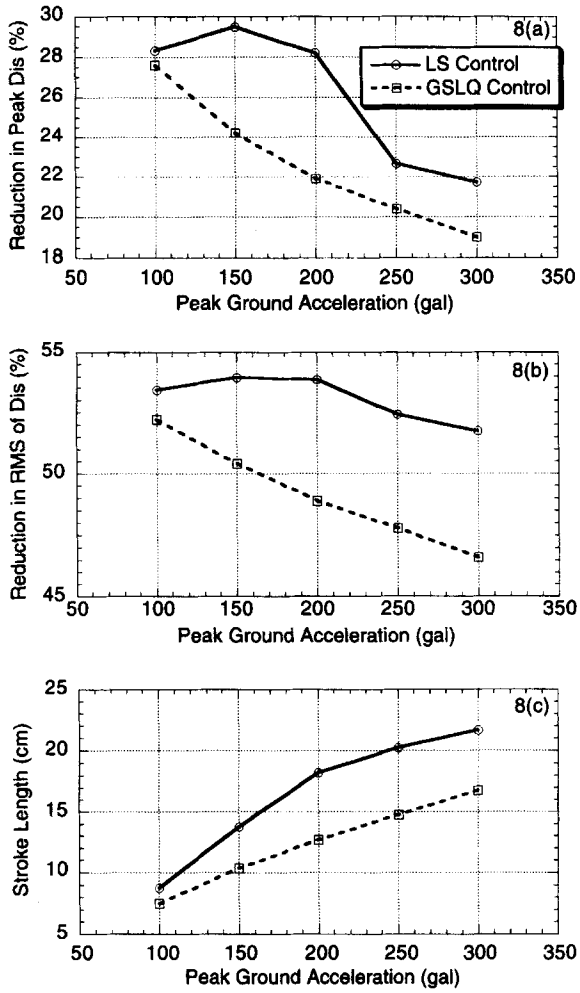

Figure 8. Performance curves for a SDOF system with ATMD subjected to the El Centro ground motion

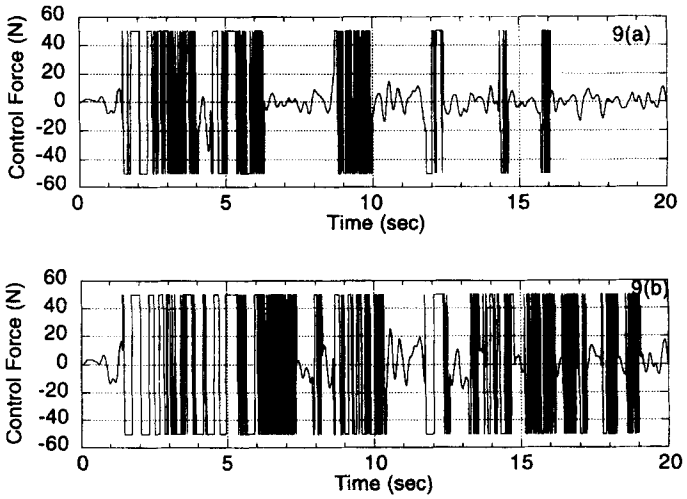

Figure 9. Control forces for a SDOF system with ATMD subjected to the El Centro ground motion with PGA values at (a) 150 and (b) 250 gal s

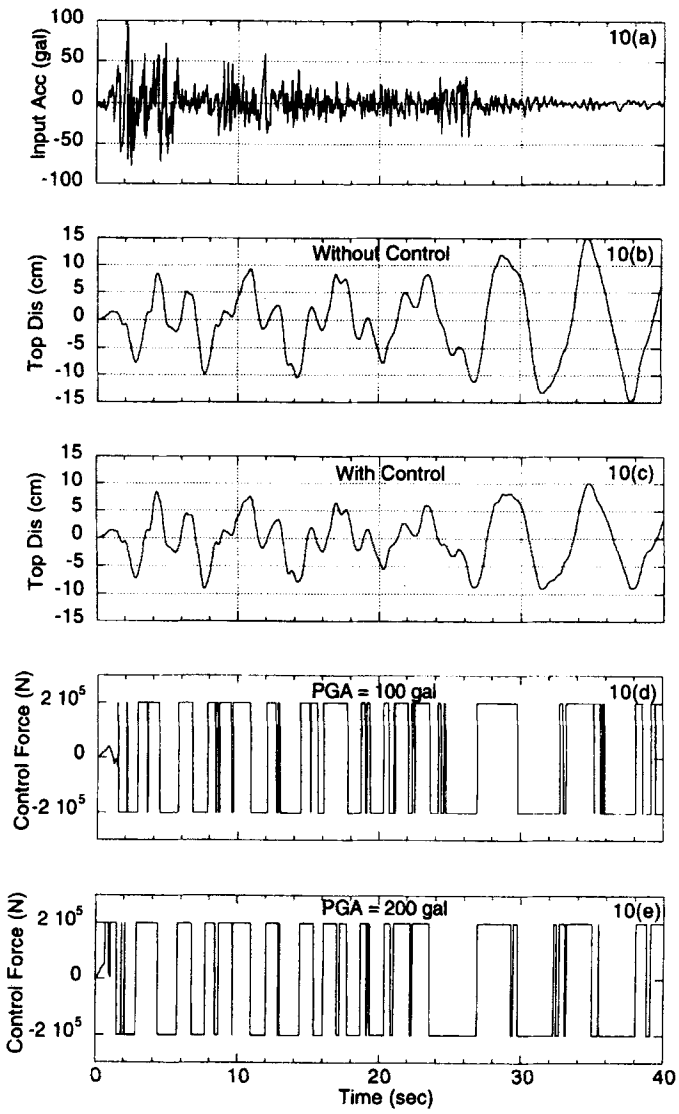

Figure 10. Input, response, and control forces for a 54-storey building with AMD subjected to the El Centro ground motion

this problem: one is, performing the LS control with the output feedback, as was done in the tall building example; and the other is to perform the LS control in the modal space, which is now under investigation.

The LS control proposed so far considers only a constraint on control force. The other constraints on the state variables such as the stroke length of added mass should be considered as well. Since directly imposing the constraints on state variables is difficult due to unpredictable excitation, several control schemes with different objectives should be implemented. For example, one control scheme controls the structure, as in this paper, and another control scheme focuses on reducing the response level of the AMD system. Then, similar to a gain-scheduled control, we can design a 'control scheme-scheduled' control, wherein at different times during a load event we would use different control schemes so as to meet the control objective and to prevent any imminent constraint violation. For this control to work, we need a good criterion to switch among the control schemes.

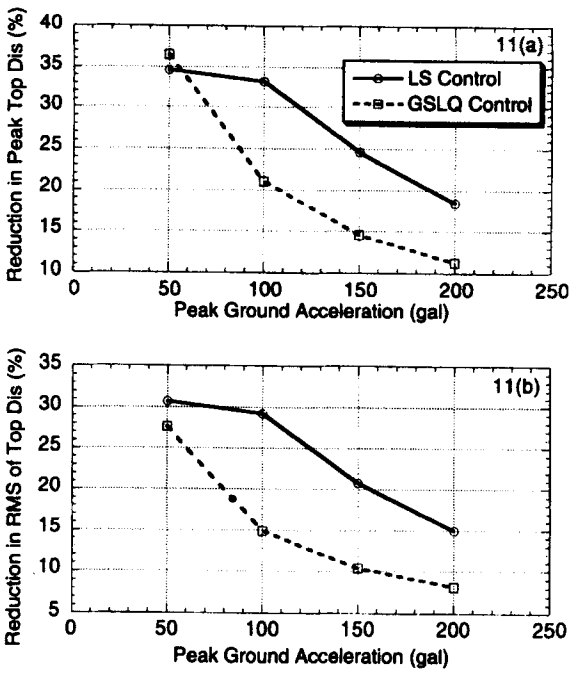

Figure 11. Performance curves for a 54-storey building with AMD subjected to the El Centro ground motion

ACKNOWLEDGEMENTS

The authors thank Taisei Corporation and Mr. Ichiro Nagashima who were instrumental in starting this research.

REFERENCES

1. T. Kobori and R. Minai, 'Nonlinear structural vibration subjected to the earthquake loading — Artificial nonlinear response process', *Trans. AIJ*, **52** (1956) (in Japanese).
2. J. T. P. Yao, 'Concept of structural control', *ASCE j. struct. div.* **98**, 1567–1573 (1972).
3. T. T. Soong, *Active Structural Control: Theory and Application*, Longman, Scientific and Technical, New York, 1990.
4. Y. Fujino, T. T. Soong and B. F. Spencer Jr., 'Structural control: Basic consepts and applications', in *ASCE proc. structures congress XIV*, Chicago, ILL, 15–18 April 1996, pp. 1277–1287.
5. J. N. Yang and F. Giannopoulos, 'Active tendon control of structures', *ASCE j. eng. mech. div.* **104**, 551–568 (1978).
6. T. Kobori, M. Takahashi, T. Nasu and N. Niwa, 'Seismic response controlled structure with active variable stiffness system', *Earthquake eng. struct. dyn.* **22**, 925–941 (1993).
7. I. Nagashima, B. Bhartia, S. Nishiyama and K. Kitazawa, 'Experimental study on active mass damper system', in *Proc. colloq. vibration control*, JSCE, Japan, 1991.
8. S. F. Masri, G. A. Bekey and T. K. Caughey, 'Optimum pulse control of flexible structures', *J. appl. mech.* **48**, 619–626 (1981).
9. S. F. Masri, G. A. Bekey and T. K. Caughey, 'On-line control of nonlinear flexible structures', *J. appl. Mech.* **49**, 877–884 (1982).
10. T. Fujita, T. Kamada and N. Masaki, 'Fundamental study of active mass damper using multistage rubber bearing and hydraulic actuator for vibration control of tall buildings (1st report, Study on control law for the active mass damper)', *Trans. Japan soc. mech. engineers* **58** (545), (1992).
11. V. I. Utkin, *Sliding Modes in Control Optimization*, Springer, New York, 1992.
12. J. N. Yang, J. C. Wu, A. K. Agrawal and Z. Li, 'Sliding mode control for seismic-excited linear and nonlinear civil engineering structures', *Technical Report, NCEER-94-0017*, 21 June 1994.
13. Z. Wu, V. Gattuli, R. C. Lin and T. T. Soong, 'Implementable control laws for peak response reductions', in *Proc. 1st world conf. on structural control*, Pasadena, U.S.A. 1994.
14. C. Johnson, 'Singular problems in optimal control', in C. Leondes (ed.), *Advances in Control Systems*, Vol. 2, Academic Press, New York, 1965, pp. 209–267.
15. A. M. Letov, 'Analytical controller design II', *Automation remote control* **21**, 389–393 (1960).
16. Chang Jen-Wei, 'A problem in the synthesis of optimal systems using the maximum principle', *Automation remote control* **22**, 1170–1176 (1961).
17. C. A. Desoer, 'The bang-bang servo problem treated by variational technique', *J. information control* **2**, 333–348 (1959).

18. H. Higashihara and B. Indrawan, 'Efficient active suppression of vibration based upon explicit treatment of actuator characteristics', *Bull. earthquake res. inst. Tokyo Univ.* **66**, 517–552 (1991).
19. A. E. Bryson and Yu-Chi Ho, *Applied Optimal Control*, Hemisphere, New York, 1975.
20. L. Meirovitch, *Dynamics and Control of structures*, Wiley, New York, 1990.
21. W. M. Wonham and C. D. Johnson, 'Optimal bang-bang control with quadratic performance index', *Trans. ASME* **86**, Ser. D, 107–115 (1964).
22. B. Friedland, 'Limiting forms of optimum stochastic linear regulators', *J. dynamic systems measurement control, Trans. ASME, ser. G* **93** (3), 134–141 (1971).
23. J. Mongkol, B. Bhartia and Y. Fujino, 'Optimal saturation control of a SDOF structure', in *Proc. 17th information system technology symp.*, AIJ, Tokyo, 1994.